



Cite this: *RSC Chem. Biol.*, 2026, 7, 216

# Sequence-specific fluorescence turn-on arises from base pairing-templated tautomerism in the tricyclic cytidine analogue <sup>DEA</sup>tC

Ana Shalamberidze, Harrison R. Pearce, Andrew L. Cooksy  and Byron W. Purse \*

Fluorescent probes for measuring the structure, dynamics, cellular localization, and biochemistry of DNA and RNA are useful for determining the regulatory mechanisms of gene expression. Intrinsically fluorescent, Watson–Crick-capable nucleobase analogues are especially powerful because they can precisely probe desired loci while minimally perturbing native nucleic acid function. Here, we study the fluorescent responses of the tricyclic pyrimidine analogue <sup>DEA</sup>tC to base pairing with adenine, guanine, and a set of noncanonical nucleobases in duplex DNA oligonucleotides. We find that single-stranded oligonucleotides containing one <sup>DEA</sup>tC exhibit up to a fivefold fluorescence increase upon hybrid duplex formation and base pairing with G, and a lesser degree of fluorescence turn-on when base pairing with inosine. Other purine nucleobases do not induce significant fluorescence turn-on. Solvent kinetic isotope effect measurements, excitation–emission matrix (EEM) analysis, and spectral comparisons indicate that fluorescence turn-on originates from base pairing-templated tautomerism. The non-emissive T-like form predominates in the single strand and in duplexes paired with A, whereas the emissive C-like tautomer is selectively stabilized upon duplex formation when paired with G. Density functional theory (DFT) calculations further support this tautomeric control model. Although base stacking influences overall brightness, it does not alter the mechanism or specificity of fluorescence turn-on. Modulation of emission through tautomeric control offers a powerful strategy for designing nucleobase analogues with base pairing-specific fluorescence responses.

Received 20th September 2025,  
Accepted 4th December 2025

DOI: 10.1039/d5cb00243e

rsc.li/rsc-chembio

## Introduction

Fluorescent nucleobase analogues (FBAs) are powerful tools for studying the structure, dynamics and chemistry of nucleic acids in isolation, in complexation with other biomolecules, and in biological environments such as cells, tissues, and even whole organisms.<sup>1–10</sup> Many applications of fluorescently labeled nucleic acids have employed traditional fluorophores such as Alexa Fluors, cyanines, and rhodamines covalently tethered to nucleic acids by flexible linkers, often installed using modified phosphoramidites.<sup>11–15</sup> Although this approach enables the selection of very bright fluorophores that absorb and emit in nearly any desired window of the optical spectrum, the flexibility of the tethers limits positional precision, allowing the dyes to sample multiple local environments and sometimes disrupt biomolecular interactions or alter cellular localization.<sup>16–20</sup> Fluorescent nucleobase analogues address these problems by substituting for native nucleobases while retaining Watson–Crick base pairing

and, in many cases, preserving the natural, global conformation of A- and B-form helices, G-quadruplexes, i-motifs, and folded RNA structures.<sup>21–29</sup> By virtue of their direct participation in base pairing and stacking, they can sense and report on both local and longer-range changes in nucleic acid conformation with high precision and sensitivity. Recent applications of FBAs have included studies on riboswitch function, measurements of the activity of base editing enzymes, imaging the uptake of exogenous mRNA and the synthesis, localization, and degradation of RNA in living cells, and the nascent area of single-molecule fluorescence studies on nucleic acids.<sup>5,9,10,28–31</sup>

While advances in the design, synthesis, and applications of FBAs are already enabling discoveries in nucleic acids biology, they are still limited by low brightness and clustering in the blue–green window of the visible spectrum.<sup>21,28</sup> The design of more red-shifted and brighter FBAs, optionally with the capacity to report on specific changes in their local environment, is a great challenge because it is difficult to understand mechanistically how the local environment—particularly base pairing and stacking—influences the excited state and the competing pathways of radiative and nonradiative relaxation.<sup>22,32–34</sup> Most

Department of Chemistry and Biochemistry, San Diego State University, San Diego, CA, USA. E-mail: [bpurse@sdsu.edu](mailto:bpurse@sdsu.edu)



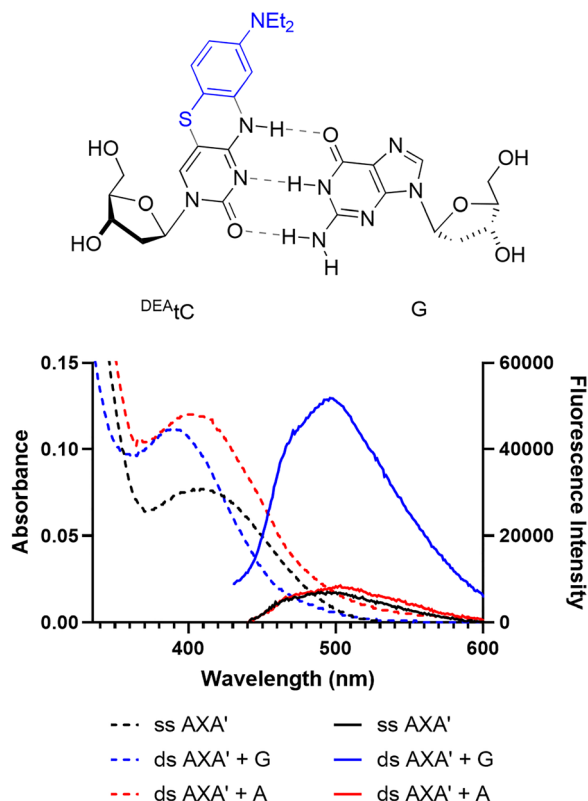


**Fig. 1** The nucleobase analogue  $^{DEA}tC$ , when incorporated into the AXA' oligonucleotide, exhibits a 5-fold increase in fluorescence intensity when base-paired with guanine, but not when base-paired with adenine (the AXA' oligonucleotide sequence is shown in Table 1). Absorption (dashed) and emission (solid) spectra were recorded in  $1\times$  PBS buffer at pH 7.4 at 37  $\mu$ M and 0.72  $\mu$ M, respectively. Emission spectra were collected using excitation at 395 nm.

FBA s are quenched by base stacking, often due to photoinduced electron transfer (PET), some retain their fluorescence, and a tiny number of known FBAs show a significant fluorescence increase.<sup>26,35–39</sup> Our group has developed and studied the tricyclic cytidine analogue  $^{DEA}tC$ , which is, to the best of our knowledge, the FBA with the greatest known increase in fluorescence intensity upon the formation of matched Watson–Crick base pairs in duplex DNA oligonucleotides and in DNA–RNA heteroduplexes (Fig. 1).<sup>26,27,39</sup> The fluorescence quantum yield of the  $^{DEA}tC$  nucleoside is  $\Phi_{em} = 0.006$  in  $1\times$  PBS buffer at pH 7.4, and this increases up to  $\Phi_{em} = 0.12$  in matched duplex DNA or  $\Phi_{em} = 0.20$  in a matched DNA–RNA heteroduplex, *i.e.* when  $^{DEA}tC$  is base paired with guanine. The magnitude of fluorescence turn-on depends to some degree on the identity of the stacked, neighboring bases, with greater influence in DNA–DNA than in DNA–RNA. No fluorescence turn-on is observed in  $^{DEA}tC:A$  base pairs or when  $^{DEA}tC$  is opposite an abasic site. While  $^{DEA}tC$  provides a powerful readout for matched base pairing that can distinguish between single nucleobases immediately upon hybridization, the mechanism that explains its specific fluorescence turn-on response is not known and base pairing partners beyond the canonical purines A and G have not been studied. Accordingly, the goal of the present study is to measure the fluorescence turn-

on response of  $^{DEA}tC$  upon hybridization and base pairing with a broad set of noncanonical nucleobases and to determine this mechanism.

## Results and discussion

We selected three neighboring nucleobase contexts and 10 base pairing partners in complementary strands to make a comprehensive assessment of how Watson–Crick-like base pairing changes the fluorescence of  $^{DEA}tC$  (Fig. 2). The 10-mer DNA oligonucleotide sequences were chosen for consistency with our past studies.<sup>26,27,39</sup> The rationale for selecting the AXA, GXC, and CXA neighboring base contexts is to cover the broadest range of neighboring base effects previously observed for  $^{DEA}tC:G$  base pairs.<sup>26,39</sup> Past studies have shown that sequence changes further removed from the nearest neighbors of an FBA have little effect on fluorescence, except when those distal changes include additional modified nucleosides well suited for effects such as photoinduced electron transfer (PET) and fluorescence resonance energy transfer (FRET).<sup>40–43</sup> The GXC sequence was found to be the brightest overall ( $\Phi_{em} = 0.12$  in dsDNA), the AXA sequences have the greatest magnitude of fluorescence turn-on from single-strand to duplex (from  $\Phi_{em} = 0.008$  to  $\Phi_{em} = 0.042$ , a 5-fold increase), and the CXA sequence is the least bright and has the smallest degree of fluorescence turn-on (from  $\Phi_{em} = 0.014$  to  $\Phi_{em} = 0.017$ , a 20% increase). For that reason, we designed this study to focus on nearest neighbor effects. We included the AXA' sequence, which lacks a 3'-terminal G, to verify that sequence changes distant from the nearest neighbors and expected to affect only overall duplex stability do not significantly alter the fluorescence response. The  $^{DEA}tC$  2'-deoxyribonucleoside and its corresponding DMTr-protected phosphoramidite were synthesized using previously published methods.<sup>26</sup> The AXA, AXA', GXC, and CXA oligonucleotides were prepared by solid-phase DNA synthesis and the complementary strands containing canonical and noncanonical nucleobases were synthesized using commercially available amidites (for details, see the SI).

First, we sought to measure the fluorescent response of each of the AXA, AXA', GXC, and CXA oligonucleotides to hybridization with all 10 complementary strands (Fig. 2 and Tables 1 and 2 and Tables S4 and S5). To ensure the completeness of duplex formation, we started with 0.72  $\mu$ M solutions of each of these  $^{DEA}tC$ -containing oligonucleotides in  $1\times$  PBS buffer at pH 7.4 and titrated in up to 2 equivalents of each complementary sequence, measuring the fluorescence change during the titration (Fig. S1–S4). For all these experiments, we observed saturation of the fluorescence change at nearly a 1:1 ratio of  $^{DEA}tC$ -containing strand to its complement, with slight variations in this ratio attributable to random experimental error. Compared with AXA, the AXA' sequence required slightly more complementary strand to reach saturation, but no significant differences were observed in its absorption, emission, or fluorescence turn-on responses, consistent with our expectation (Fig. S2 and S4 and Fig. S10–S13). Further addition of the complementary strands beyond the 1:1



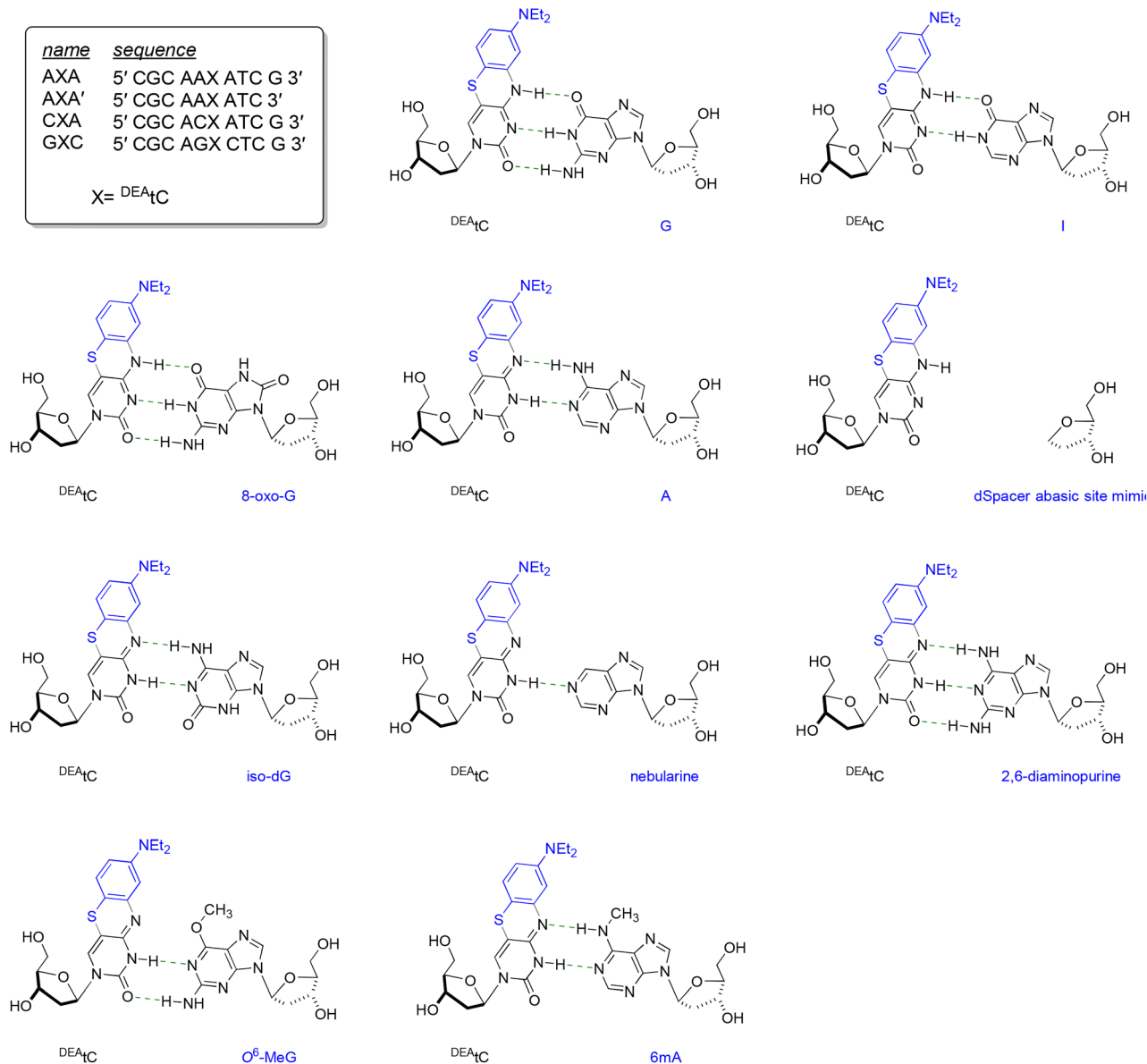


Fig. 2 Sequences of the AXA, AXA', GXC, and CXA oligonucleotides, which contain DEATC, and the structure of DEATC base pairs used in this study.

ratio resulted in little change in fluorescence. As expected for these sequences, an equilibrium of matched duplex formation is attained at ambient temperature; the use of an annealing protocol resulted in no significant differences.

The resulting data shows that DEATC's fluorescence turn-on response is unique to base pairing with guanine-like partners that would be expected to favor Watson-Crick base pairing with a cytosine-like tautomer of DEATC (Fig. 3 and Fig. S10). Fluorescence turn-on is greatest for base pairing with guanine, as previously observed, and we detect a significant but lesser degree of fluorescence turn-on in DEATC:inosine base pairs, which lack the exocyclic amino group N2 of guanine. 8-Oxo-G has the same Watson-Crick edge as guanine, but does not induce a fluorescence turn-on when base-paired with DEATC. These results are consistent for the AXA', AXA, GXC, and CXA

sequences, with the latter showing only small fluorescence changes. Other base pairing partners, which include those expected to favor a thymine-like tautomer of DEATC, the formation of wobble base pairs, or, like nebularine, have greatly reduced capacity to form hydrogen bonds, show no significant fluorescence turn-on, a result also observed when DEATC is present opposite an abasic site.

Having observed that DEATC's fluorescence turn-on is unique to base pairing with certain G-like partners, we next sought to determine the mechanism that would explain this specificity. Our past structural determination work using <sup>1</sup>H NMR spectroscopy has shown that duplex DNA oligonucleotides containing a single substitution of DEATC for C retain the normal B-form conformation and that DEATC engages in Watson-Crick base pairing and base stacking similar to that of cytosine, but with



**Table 1** Steady-state fluorescence measurements of <sup>DEA</sup>tC in single- and double-stranded DNA oligonucleotides for the AXA' sequence 5'-CGCAAXATC-3', where X = <sup>DEA</sup>tC. Absorption and emission measurements were recorded in 1× PBS buffer at pH 7.4 at 37 μM and 0.72 μM, respectively. Emission spectra were collected using excitation at 395 nm

Sequence name	$\lambda_{\max}$ Absorption/nm	$\lambda_{\max}$ Excitation/nm	$\lambda_{\max}$ Emission/nm	Fluorescence intensity change <sup>a</sup>
ss AXA' <sup>b</sup>	409	386	496	n/a
ds G <sup>c</sup>	390	397	494	5.53
ds A	401	395	494	1.34
ds I	391	394	493	3.44
ds 8oxoG	392	396	495	1.66
ds dSpacer	414	389	494	0.84

<sup>a</sup> Fluorescence intensity change is reported as the ratio of the integrated emission intensity of each duplex with respect to ss AXA' using 395 nm excitation. <sup>b</sup> ss = single-stranded. <sup>c</sup> ds G refers to the matched complementary duplex with <sup>DEA</sup>tC base paired with G; other duplex names follow this convention.

**Table 2** Steady-state fluorescence measurements of <sup>DEA</sup>tC in single- and double-stranded DNA oligonucleotides for the GXC sequence 5'-CGCA GXCTCG-3', where X = <sup>DEA</sup>tC. Absorption and emission measurements were recorded in 1× PBS buffer at pH 7.4 at 37 μM and 0.72 μM, respectively. Emission spectra were collected using excitation at 395 nm

Sequence name	$\lambda_{\max}$ Absorption/nm	$\lambda_{\max}$ Excitation/nm	$\lambda_{\max}$ Emission/nm	Fluorescence intensity change <sup>a</sup>
ss GXC <sup>b</sup>	409	396	499	n/a
ds G <sup>c</sup>	390	396	499	5.42
ds A	415	397	500	0.72
ds I	391	396	499	3.24
ds 8oxoG	392	397	498	1.53
ds dSpacer	416	397	498	0.32

<sup>a</sup> Fluorescence intensity change is reported as the ratio of the integrated emission intensity of each duplex with respect to ss GXC using 395 nm excitation. <sup>b</sup> ss = single-stranded. <sup>c</sup> ds G refers to the matched complementary duplex with <sup>DEA</sup>tC base paired with G; other duplex names follow this convention.

extended  $\pi$  stacking.<sup>39</sup> Recognizing that the fluorescence quantum yield of <sup>DEA</sup>tC is lowest as a free nucleoside and that engagement in a specific configuration of Watson-Crick-edge hydrogen bonding is crucial, we first hypothesized that desolvation and hydrogen bonding of <sup>DEA</sup>tC in the duplex protects this FBA from excited-state proton transfer (ESPT), a prominent fluorescence quenching mechanism, thereby inducing turn-on. To test this hypothesis, we measured the influence of buffer deuteration on the fluorescence intensity of the single-stranded GXC oligonucleotide and the hybrid duplexes with <sup>DEA</sup>tC base paired with G or opposite the dSpacer abasic site mimic, a 1',2'-dideoxyribose (Fig. 4). For these experiments, we measured the fluorescence intensity of the single-stranded and duplex oligonucleotides in replicate, using 1× PBS buffer at pH 7.4 and an equivalent buffer prepared in D<sub>2</sub>O. We found that the brightness in deuterated buffer ÷ the brightness in regular buffer = 3.23 for the GXC ssDNA oligonucleotide. Because buffer deuteration slows the rate of ESPT, a kinetic isotope effect, we conclude that ESPT is a significant quenching mechanism of <sup>DEA</sup>tC's fluorescence in the GXC oligonucleotide.

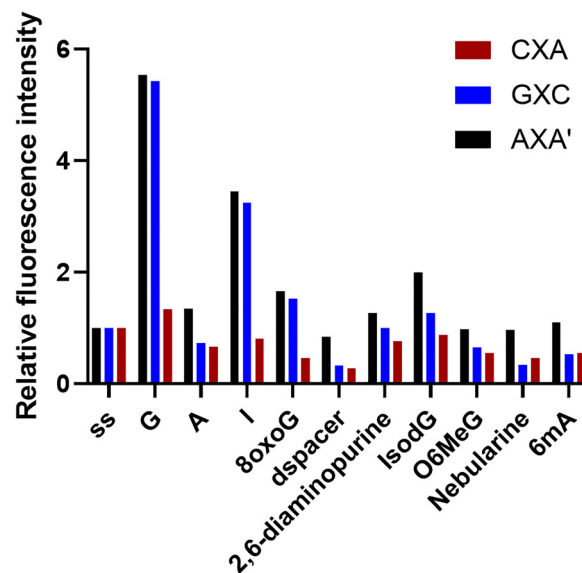


**Fig. 3** Relative fluorescence intensity of the single-stranded (ss) CXA, GXC, and AXA' oligonucleotides and their hybrid duplexes with G, A, and noncanonical nucleobases. Fluorescence intensity change is reported as the ratio of the integrated emission intensity of each duplex with respect to the <sup>DEA</sup>tC-containing single strand, using 395 nm excitation.

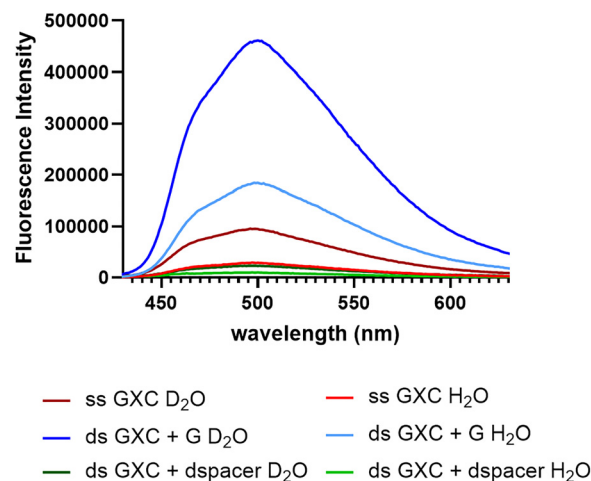


**Fig. 4** Fluorescence intensity comparison of the GXC sequence (0.72 μM) as a single-stranded oligonucleotide and in hybrid duplexes with <sup>DEA</sup>tC base paired with G or opposite the dSpacer abasic site mimic in normal (H<sub>2</sub>O; light colors) vs. deuterated (D<sub>2</sub>O; dark colors) 1× PBS buffer, pH 7.4. Excitation was at 395 nm.

When repeating these experiments using the GXC duplexes with <sup>DEA</sup>tC:G and <sup>DEA</sup>tC:dSpacer base pairs, respectively, we found that the fluorescence intensity ratio for samples in deuterated vs. regular buffer ratio is 2.40 for the former and 2.20 for the latter. Duplex formation attenuates the rate of quenching by ESPT, but this attenuation does not depend on base pairing. Accordingly, the hypothesis is disproved. The specificity of <sup>DEA</sup>tC's fluorescence turn-on is not the result of the special ability of a G:C-like configuration of Watson-Crick hydrogen bonding to slow the rate of ESPT.



Desolvation of  $^{DEA}tC$  when base paired and stacked is, by itself, an insufficient mechanism to explain the specificity of fluorescence turn-on, because one would expect a similar degree of desolvation in many of the base pairing configurations of  $^{DEA}tC$  that do not exhibit fluorescence turn-on (Fig. 3).

Next, we hypothesized that tautomerism of  $^{DEA}tC$  might explain this specificity.  $^{DEA}tC$  is the diethylamino derivative of  $tC$ , a well characterized fluorescent cytidine analogue that has nearly the same fluorescent brightness as a free nucleoside, in single-stranded, and in duplex oligonucleotides.<sup>44</sup> While we have previously reported  $^{DEA}tC$ 's fluorescence turn-on response upon hybrid duplex formation,<sup>26,27,39</sup> its tautomerism has not yet been experimentally assessed. Tautomerism is established as a significant determinant of the photophysical properties of some fluorescent nucleobase analogues,<sup>22,45,46</sup> and although a reported ABN study revealed a modest base pairing-templated tautomerism effect in duplex DNA,<sup>29</sup> to our knowledge it has not been shown to serve as the dominant mechanism driving fluorescence changes in duplex oligonucleotides. A previous study examined the incorporation of  $d(tC)TP$  and  $d(tC^O)TP$ , the triphosphate forms of the related cytidine analogues  $tC$  and  $tC^O$ , by human DNA polymerase  $\alpha$  and the Klenow fragment.<sup>47</sup> These reactions showed increased misincorporation opposite adenine, attributed to the greater tendency of  $tC$  and  $tC^O$  to interconvert between tautomers compared with natural cytosine. To investigate how tautomerism of  $^{DEA}tC$  might contribute to its fluorescence turn-on specificity, we compared its absorption and excitation spectra as a function of hybridization (Fig. 5). These measurements are informative because the absorption spectrum reflects all species with appreciable extinction coefficients at each wavelength,

whereas the excitation spectrum isolates the subset of those species that are emissive at the monitored wavelength. Accordingly, significant differences between absorption and excitation spectra indicate the presence of multiple ground-state species, only some of which are fluorescent (or, more properly, exhibit differing fluorescence) upon excitation.

We recorded absorption and excitation spectra for the AXA' sequence as a single-stranded oligonucleotide and in hybrid duplexes with G, A, I, 8-oxo-G, and dSpacer (1',2'-dideoxyribose). The excitation spectra were collected using 500 nm as the emission wavelength, close to  $\lambda_{max}$  for the fluorescence. By plotting these spectra together, clear differences are observed, depending on  $^{DEA}tC$ 's base pairing partner (data for the AXA' sequence are shown in Fig. 5; very similar data are observed for GXC as shown in Fig. S5). First, we note that all excitation spectra have a maximum near 395 nm and a shoulder at 370 nm, with the exception of AXA':dSpacer, which is slightly more absorbing at 370 nm and less absorbing at 395 nm. The maximum at 395 nm—and the overall appearance of the excitation spectra—matches the absorption spectra when  $^{DEA}tC$  is base paired with G, I, and 8-oxo-G, all configurations that are expected to strongly reinforce  $^{DEA}tC$ 's C-like hydrogen bonding configuration in Watson–Crick base pairing. However, the absorption and excitation spectra do not match for the single-stranded AXA' oligonucleotide and in hybrid duplexes wherein  $^{DEA}tC$  is base paired with A and dSpacer, configurations that would favor  $^{DEA}tC$ 's T-like hydrogen bonding configuration in Watson–Crick base pairing or would not template its tautomerism, respectively. Notably, both these hybrid duplexes have less fluorescence intensity than the single-stranded AXA' oligonucleotide and  $\lambda_{max,abs}$  is red-shifted by 9 nm and 18 nm, respectively, without an accompanying change in  $\lambda_{max}$  for excitation. Rather, the excitation spectra closely resemble those observed when  $^{DEA}tC$  is base paired with G.

These results can be explained by a model wherein  $^{DEA}tC$ 's tautomerism, which is templated by base pairing, is the primary control of its fluorescence. When  $^{DEA}tC$  is base paired with G or inosine, its cytosine-like tautomer is stabilized and is the predominant species present. The absorption and excitation spectra match, and the greatest fluorescent brightness is observed. In contrast, when  $^{DEA}tC$  is base paired with A, the thymine-like tautomer is templated and is the major species present, which is indicated by the red-shifted  $\lambda_{max,abs}$ . This tautomer is nearly non-emissive. A minor population of the C-like tautomer persists, explaining the retention of an excitation spectrum similar to those observed when  $^{DEA}tC$  is base paired with G or inosine, and a low degree of residual fluorescence. The single-stranded AXA' oligonucleotide has a similar mismatch between its absorption and emission spectra with the former red-shifted, indicating that the T-like tautomer is favored and explaining the low  $\Phi_{em} = 0.008$ .<sup>26</sup>

To validate this model, we recorded emission spectra across excitation wavelengths from 350–450 nm and constructed excitation–emission matrices (EEMs) for the single-stranded AXA' oligonucleotide, the AXA':A duplex, and the AXA':G duplex (Fig. 6, shown as both 3D surface and contour plots; complementary 2D plots and data for AXA are shown in the Fig. S12 and S13). EEM analysis sensitively reveals the presence of multiple

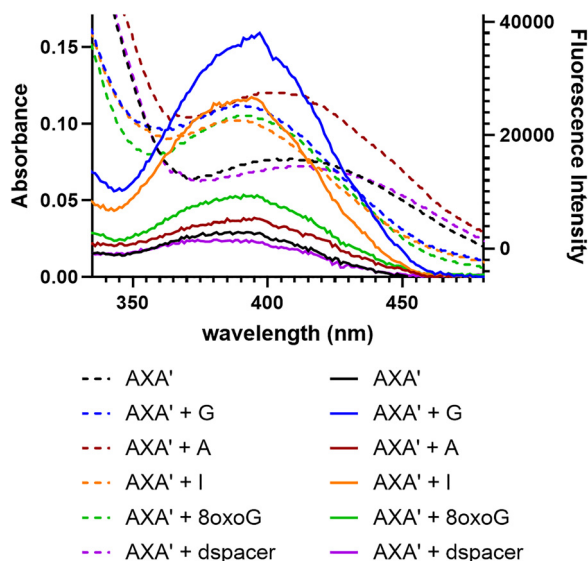


Fig. 5 Absorption (dashed) and excitation (solid; collected using an emission wavelength of 500 nm) of the single-stranded (ss) AXA' oligonucleotide and hybrid duplexes with  $^{DEA}tC$  base paired with G, A, I, 8-oxo-G, and dSpacer (1',1'-dideoxyribose). Absorption and excitation spectra were recorded in  $1\times$  PBS buffer at pH 7.4 at 37  $\mu$ M and 0.72  $\mu$ M, respectively. Excitation spectra were collected by monitoring emission at 500 nm.



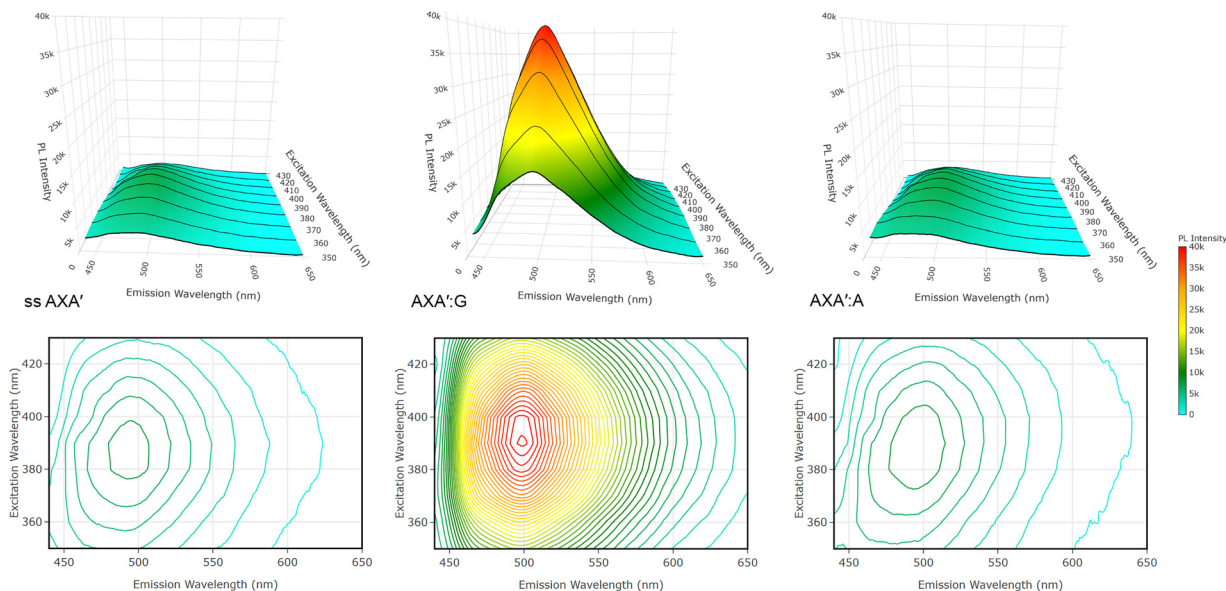


Fig. 6 Excitation–emission matrix plots for single-stranded AXA', the AXA':G duplex, and the AXA':A duplex. Data were collected in  $1\times$  PBS buffer at pH 7.4 at and  $0.72\ \mu\text{M}$  AXA' strand.

emissive species and how their relative populations shift in response to environmental changes, in this case those arising from base pairing. Although quantitative deconvolution is limited by spectral overlap between the C- and T-like tautomers of  $\text{DEA}_{\text{tC}}$ , the EEMs clearly show tautomeric shifts induced by base pairing. The single-stranded AXA' construct exhibits low overall fluorescence, with a main emission at 499 nm (C-like tautomer) and a distinct shoulder at 463 nm (T-like tautomer). In this unpaired state, the non-emissive T-like tautomer predominates, but the minor C-like species dominates the observed spectrum owing to its much higher intrinsic fluorescence. Upon duplex formation with adenine, base pairing stabilizes and templates the T-like tautomer, enhancing the 463 nm feature and producing stronger contours in the lower-left quadrant of the EEM plot. In contrast, base pairing with guanine templates the emissive C-like tautomer and suppresses the T-like tautomer almost completely, resulting in the pronounced fluorescence enhancement characteristic of  $\text{DEA}_{\text{tC}}$  turn-on.

This model of tautomerism-controlled fluorescence turn-on explains the fluorescent response to all base pairing partners except 8-oxo-G, which templates the C-like tautomer through Watson–Crick base pairing but does not elicit a fluorescence turn-on. The templating of the C-like tautomer is indicated by the matched absorption and excitation spectra with  $\lambda_{\text{max}} = 395\ \text{nm}$ , and in this special case the lack of a significant fluorescence turn-on is the result of quenching by photo-induced electron transfer (PET). 8-Oxo-G has been previously reported to be a potent quencher of other FBAs by this mechanism, which is enabled by its electron deficiency as compared with guanine.<sup>48,49</sup> Inosine is less able to stably template the C-like tautomer of  $\text{DEA}_{\text{tC}}$  because its base pair lacks a hydrogen bond; the fluorescence turn-on is accordingly attenuated. The other base pairing partners studied favor the T-like tautomer of

$\text{DEA}_{\text{tC}}$ , explaining the low fluorescence emission in these hybrid duplexes.

The  $\text{DEA}_{\text{tC}}$  nucleoside is similarly non-emissive in Milli-Q water and  $1\times$  PBS buffer at pH 7.4. Although both spectra are blue-shifted with respect to those observed in single-stranded and duplex oligonucleotides, a discrepancy is again observed between the absorption and excitation spectra, with the latter blue-shifted as compared with the former (Fig. 7). The low fluorescence emission of the  $\text{DEA}_{\text{tC}}$  nucleoside can be explained by significant adoption of the T-like tautomer in aqueous solution and its greater solvation as compared with the environment in oligonucleotides. The relative blue-shift of its absorption and excitation spectra with respect to those observed in oligonucleotides indicates that base stacking stabilizes the excited state relative to the ground state.

Computational studies further support this model of fluorescence turn-on. We carried out B3LYP-D3(BJ)/cc-pVDZ/SMD<sup>50–56</sup>

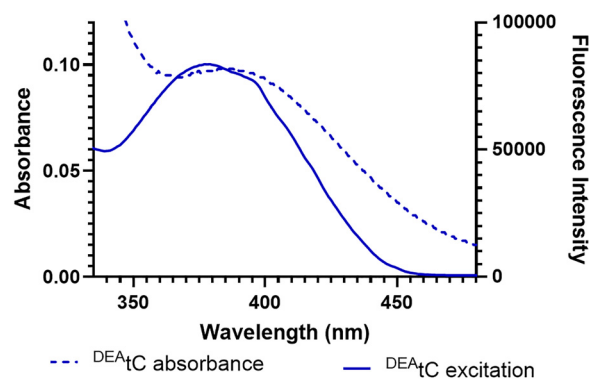


Fig. 7 Absorption (dashed) and excitation (solid; collected using an emission wavelength of 500 nm) of the  $\text{DEA}_{\text{tC}}$  2'-deoxyribonucleoside in Milli-Q water.  $\lambda_{\text{max,abs}} = 377\ \text{nm}$  and  $\lambda_{\text{max,ex}} = 385\ \text{nm}$ .



geometry optimizations of <sup>DEA</sup>tC base paired with guanine, inosine and adenine using an AXA trimer duplex constrained in the normal B-form geometry, with water as the implicit solvent. Following geometry optimization, we truncated the base pairs at the 1'-carbon, replacing the phosphoribose backbone with hydrogens, frozen in position. Absorption spectra were predicted with the TD-CAM-B3LYP<sup>57</sup> method and cc-pVDZ, aug-cc-pVDZ, and aug-cc-pVTZ basis sets. Relative B3LYP energies of the monomeric C-like and T-like tautomers differed by less than 0.1 kcal mol<sup>-1</sup> when expanding the basis set from aug-cc-pVDZ to aug-cc-pVTZ basis sets, so B3LYP/aug-cc-pVDZ calculations were used for single-point energy calculations of the relative ground state energies in the dimer and base stacked systems. Similarly, absorption wavelengths of the monomers differed by less than 1 nm between the aug-cc-pVDZ and aug-cc-pVTZ basis sets. While B3LYP has been a robust method for geometry optimizations, the long-range corrections present in the CAM-B3LYP functional make CAM-B3LYP a more accurate method over a wide range of electronic transitions.<sup>58,59</sup>

Comparing the electronic energies of the two tautomers, the C-like tautomer is calculated to be more stable than the T-like tautomer even as a monomer, but only by 5 kcal mol<sup>-1</sup>. An exhaustive benchmark study of DFT calculations found an RMSD of 5.50 kcal mol<sup>-1</sup> for B3LYP isomerization energies,<sup>60</sup> and it is unsurprising that the experimental evidence indicates that the T-like free nucleoside is more stable than the C-like. Upon formation of the base-paired complexes with inosine, our calculations predict a substantial 28 kcal mol<sup>-1</sup> stabilization of the C-like tautomer relative to T-like, well outside the expected error range and strongly supporting the hypothesis that base-pairing preferentially templates the <sup>DEA</sup>tC to the C-like form. We could not make a comparable analysis for base pairing with guanine because its stronger templating capacity caused self-consistent field (SCF) convergence problems when modeling the base pair between the T-like tautomer of <sup>DEA</sup>tC and guanine.

The wavelengths of the trimer absorption spectra are predicted to be much shorter than experimentally observed (Table 3), but the calculated wavelength differences between C-like and T-like tautomer complexes replicate the significant red-shift observed in experiment when comparing C-like forms (342–356 nm) to T-like forms (364–378 nm). Although superior methods will be needed to more accurately predict the spectra

quantitatively, these results again indicate that base-pairing with G is templating the <sup>DEA</sup>tC into the C-like tautomer.

## Conclusions

In this study, we examined how the fluorescent nucleobase analogue <sup>DEA</sup>tC responds to base pairing with a series of purine partners in duplex DNA oligonucleotides. The strongest response is to base-pairing with G, which affords up to a 5-fold fluorescence turn-on as compared with the <sup>DEA</sup>tC-containing single-stranded oligonucleotide. Inosine induces up to a 3-fold fluorescence turn-on and there is little response to base pairing with other purines. Solvent kinetic isotope effects show that excited-state proton transfer is a significant quenching mechanism of <sup>DEA</sup>tC, which limits its brightness, but this mechanism is not influenced by base pairing and its attenuation in duplexes cannot explain the selectivity and magnitude of fluorescence turn-on. Instead, drawing on differences revealed by absorption and excitation spectra together with excitation–emission matrix analysis, and supported by DFT calculations, we find that <sup>DEA</sup>tC's low fluorescence as a free nucleoside arises from its predominantly thymine-like tautomeric state. Base pairing in hybrid duplexes can shift this equilibrium. When paired with guanine or inosine, the cytosine-like, emissive tautomer is favored, producing fluorescence turn-on. The effect is stronger with guanine because its triply hydrogen-bonded base pair with <sup>DEA</sup>tC provides a more powerful tautomeric templating influence. In contrast, base pairs that stabilize <sup>DEA</sup>tC's T-like tautomer exhibit low fluorescence. Only the absence of fluorescence induction by 8-oxo-G falls outside this framework, though it can be accounted for by the well-known efficiency of 8-oxo-G as a PET quencher. In addition, the computational model accurately predicts both the enhanced stability of the C-like tautomer upon base pairing with guanine and inosine and the blue-shift of the C-like monomer absorption spectrum relative to the T-like tautomer. Accordingly, <sup>DEA</sup>tC's fluorescence turn-on property is a highly specific result of templated tautomerism induced by base pairing. This fluorescence turn-on mechanism complements the more-studied approach to induced fluorescence turn-on in duplex nucleic acids, wherein the fluorophore is rigidified and bond rotation is restricted by local structure.<sup>38,61</sup> In our opinion, further development of nucleoside analogues designed for fluorescence turn-on by induced tautomerism presents an exciting opportunity to impart useful probing capabilities to this powerful class of molecular sensors.

**Table 3** CAM-B3LYP/aug-cc-pVDZ/SMD//B3LYP/cc-pVDZ calculated maximum absorption wavelengths for <sup>DEA</sup>tC

Configuration	Calculated $\lambda_{\text{max,abs}}$ /nm for the C-like tautomer	Calculated $\lambda_{\text{max,abs}}$ /nm for the T-like tautomer
<sup>DEA</sup> tC nucleobase	342	378
<sup>DEA</sup> tC in single-stranded AXA	356	378
<sup>DEA</sup> tC in AXA and base paired with G	356	—
<sup>DEA</sup> tC in AXA and base paired with I	353	364
<sup>DEA</sup> tC in AXA and base paired with A	—	377

## Author contributions

AS: methodology, visualization, writing – review & editing; HRP: formal analysis, methodology, visualization, writing – review & editing; ALC: conceptualization, formal analysis, supervision, validation, writing – review & editing; BWP: conceptualization, data curation, methodology, project administration, resources, supervision, validation, writing – original draft, writing – review & editing.



## Conflicts of interest

There are no conflicts to declare.

## Data availability

The data supporting the findings of this study are available within the paper and its supplementary information (SI). Supplementary information: experimental procedures, sequences of oligonucleotides, fluorescence titration data, absorption/excitation/emission spectra, supporting tables and figures, and computational methods with optimized geometries and calculated absorption data. See DOI: <https://doi.org/10.1039/d5cb00243e>.

Output files from the computational work are available at the ioChem-BD database DOI: <https://doi.org/10.19061/iochem-bd-6-576>.

## Acknowledgements

This material is based upon work supported by the National Science Foundation under Grants No. CHE-2102642 and CHE-2453516, awarded to B.W.P. This work used Expanse at the San Diego Supercomputer Center through allocation CHE250077 from the Advanced Cyberinfrastructure Coordination Ecosystem: Services & Support (ACCESS) program, which is supported by U.S. National Science Foundation grants #2138259, #2138286, #2138307, #2137603, and #2138296.<sup>62</sup>

## References

- 1 N. Grytsyk, L. Richert, P. Didier, D. Dziuba, S. Ciaco, V. Mazzoleni, T. Lequeu, M. Mori, Y. Tor, L. Martinez-Fernandez, R. Improta and Y. Mély, Thienoguanosine, a Unique Non-Perturbing Reporter for Investigating Rotational Dynamics of DNA Duplexes and Their Complexes with Proteins, *Int. J. Biol. Macromol.*, 2022, **213**, 210–225, DOI: [10.1016/j.ijbiomac.2022.05.162](https://doi.org/10.1016/j.ijbiomac.2022.05.162).
- 2 W. Copp, A. Karimi, T. Yang, A. Guarné and N. W. Luedtke, Fluorescent Molecular Rotors Detect O6-Methylguanine Dynamics and Repair in Duplex DNA, *Chem. Commun.*, 2024, **60**(9), 1156–1159, DOI: [10.1039/D3CC04782B](https://doi.org/10.1039/D3CC04782B).
- 3 K. B. Steinbuch, D. Cong, A. J. Rodriguez and Y. Tor, Emissive Guanosine Analog Applicable for Real-Time Live Cell Imaging, *ACS Chem. Biol.*, 2024, **19**(8), 1836–1841, DOI: [10.1021/acscchembio.4c00398](https://doi.org/10.1021/acscchembio.4c00398).
- 4 K. B. Steinbuch, M. Bucardo and Y. Tor, Emissive Alkylated Guanine Analogs as Probes for Monitoring O6-Alkylguanine-DNA-Transferase Activity, *ACS Omega*, 2024, **9**(34), 36778–36786, DOI: [10.1021/acsomega.4c05700](https://doi.org/10.1021/acsomega.4c05700).
- 5 D. Wang, A. Shalamberidze, A. E. Arguello, B. W. Purse and R. E. Kleiner, Live-Cell RNA Imaging with Metabolically Incorporated Fluorescent Nucleosides, *J. Am. Chem. Soc.*, 2022, **144**(32), 14647–14656, DOI: [10.1021/jacs.2c04142](https://doi.org/10.1021/jacs.2c04142).
- 6 J. A. Riback, J. M. Eeftens, D. S. W. Lee, S. A. Quinodoz, A. Donlic, N. Orlovsky, L. Wiesner, L. Beckers, L. A. Becker, A. R. Strom, U. Rana, M. Tolbert, B. W. Purse, R. Kleiner, R. Kriwacki and C. P. Brangwynne, Viscoelasticity and Advective Flow of RNA Underlies Nucleolar Form and Function, *Mol. Cell*, 2023, **83**(17), 3095–3107, DOI: [10.1016/j.molcel.2023.08.006.e9](https://doi.org/10.1016/j.molcel.2023.08.006.e9).
- 7 T. Triemer, A. Messikommer, S. M. K. Glasauer, J. Alzeer, M. H. Paulisch and N. W. Luedtke, Superresolution Imaging of Individual Replication Forks Reveals Unexpected Prodrug Resistance Mechanism, *Proc. Natl. Acad. Sci. U. S. A.*, 2018, 201714790, DOI: [10.1073/pnas.1714790115](https://doi.org/10.1073/pnas.1714790115).
- 8 V. N. Schreier, M. O. Loehr, E. Lattmann and N. W. Luedtke, Active Uptake and Trafficking of Nucleoside Triphosphates In Vivo, *ACS Chem. Biol.*, 2022, **17**(7), 1799–1810, DOI: [10.1021/acscchembio.2c00153](https://doi.org/10.1021/acscchembio.2c00153).
- 9 T. Baladi, J. R. Nilsson, A. Gallud, E. Celauro, C. Gasse, F. Levi-Acobas, I. Sarac, M. R. Hollenstein, A. Dahlén, E. K. Esbjörner and L. M. Wilhelmsson, Stealth Fluorescence Labeling for Live Microscopy Imaging of mRNA Delivery, *J. Am. Chem. Soc.*, 2021, **143**(14), 5413–5424, DOI: [10.1021/jacs.1c00014](https://doi.org/10.1021/jacs.1c00014).
- 10 A. Sun, C. Gasser, F. Li, H. Chen, S. Mair, O. Krasheninina, R. Micura and A. Ren, SAM-VI Riboswitch Structure and Signature for Ligand Discrimination, *Nat. Commun.*, 2019, **10**(1), 5728, DOI: [10.1038/s41467-019-13600-9](https://doi.org/10.1038/s41467-019-13600-9).
- 11 N. Kretschy and M. M. Somoza, Comparison of the Sequence-Dependent Fluorescence of the Cyanine Dyes Cy3, Cy5, DyLight DY547 and DyLight DY647 on Single-Stranded DNA, *PLoS One*, 2014, **9**(1), e85605, DOI: [10.1371/journal.pone.0085605](https://doi.org/10.1371/journal.pone.0085605).
- 12 M. Hocek and M. Fojta, Cross-Coupling Reactions of Nucleoside Triphosphates Followed by Polymerase Incorporation. Construction and Applications of Base-Functionalized Nucleic Acids, *Org. Biomol. Chem.*, 2008, **6**(13), 2233–2241, DOI: [10.1039/B803664K](https://doi.org/10.1039/B803664K).
- 13 N. Ramsay, A.-S. Jemth, A. Brown, N. Crampton, P. Dear and P. Holliger, CyDNA: Synthesis and Replication of Highly Cy-Dye Substituted DNA by an Evolved Polymerase, *J. Am. Chem. Soc.*, 2010, **132**(14), 5096–5104, DOI: [10.1021/ja909180c](https://doi.org/10.1021/ja909180c).
- 14 L. M. Hall, M. Gerowska and T. Brown, A Highly Fluorescent DNA Toolkit: Synthesis and Properties of Oligonucleotides Containing New Cy3, Cy5 and Cy3B Monomers, *Nucleic Acids Res.*, 2012, **40**(14), e108, DOI: [10.1093/nar/gks303](https://doi.org/10.1093/nar/gks303).
- 15 Z. Zhu, J. Chao, H. Yu and A. S. Waggoner, Directly Labeled DNA Probes Using Fluorescent Nucleotides with Different Length Linkers, *Nucleic Acids Res.*, 1994, **22**(16), 3418–3422.
- 16 K. Jahnke, H. Grubmüller, M. Igaev and K. Göpfrich, Choice of Fluorophore Affects Dynamic DNA Nanostructures, *Nucleic Acids Res.*, 2021, **49**(7), 4186–4195, DOI: [10.1093/nar/gkab201](https://doi.org/10.1093/nar/gkab201).
- 17 J. Ouellet, S. Schorr, A. Iqbal, T. J. Wilson and D. M. J. Lilley, Orientation of Cyanine Fluorophores Terminally Attached to DNA via Long, Flexible Tethers, *Biophys. J.*, 2011, **101**(5), 1148–1154, DOI: [10.1016/j.bpj.2011.07.007](https://doi.org/10.1016/j.bpj.2011.07.007).
- 18 R. Fischer, T. Waizenegger, K. Köhler and R. Brock, A Quantitative Validation of Fluorophore-Labelled Cell-Permeable Peptide Conjugates: Fluorophore and Cargo Dependence of Import, *Biochim. Biophys. Acta, Biomembr.*, 2002, **1564**(2), 365–374, DOI: [10.1016/S0005-2736\(02\)00471-6](https://doi.org/10.1016/S0005-2736(02)00471-6).
- 19 C. A. Puckett and J. K. Barton, Fluorescein Redirects a Ruthenium–Octaarginine Conjugate to the Nucleus, *J. Am.*



- Chem. Soc.*, 2009, **131**(25), 8738–8739, DOI: [10.1021/ja9025165](https://doi.org/10.1021/ja9025165).
- 20 M. R. Herling and I. J. Dmochowski, Ratiometric, pH-Sensitive Probe for Monitoring siRNA Delivery, *J. Am. Chem. Soc.*, 2023, **145**(17), 9417–9422, DOI: [10.1021/jacs.3c01032](https://doi.org/10.1021/jacs.3c01032).
- 21 W. Xu, K. M. Chan and E. T. Kool, Fluorescent Nucleobases as Tools for Studying DNA and RNA, *Nat. Chem.*, 2017, **9**(11), 1043–1055, DOI: [10.1038/nchem.2859](https://doi.org/10.1038/nchem.2859).
- 22 D. Dziuba, P. Didier, S. Ciaco, A. Barth, C. A. M. Seidel and Y. Mély, Fundamental Photophysics of Isomorphous and Expanded Fluorescent Nucleoside Analogues, *Chem. Soc. Rev.*, 2021, **50**(12), 7062–7107, DOI: [10.1039/D1CS00194A](https://doi.org/10.1039/D1CS00194A).
- 23 P. T. Ludford III, S. Yang, M. S. Bucardo and Y. Tor, A New Variant of Emissive RNA Alphabets, *Chem. – Eur. J.*, 2022, **28**(13), e202104472, DOI: [10.1002/chem.202104472](https://doi.org/10.1002/chem.202104472).
- 24 S. Hirashima, J. H. Han, H. Tsuno, Y. Tanigaki, S. Park and H. Sugiyama, New Size-Expanded Fluorescent Thymine Analogue: Synthesis, Characterization, and Application, *Chem. – Eur. J.*, 2019, **25**(42), 9913–9919, DOI: [10.1002/chem.201900843](https://doi.org/10.1002/chem.201900843).
- 25 Y. Saito and R. H. E. Hudson, Base-Modified Fluorescent Purine Nucleosides and Nucleotides for Use in Oligonucleotide Probes, *J. Photochem. Photobiol., C*, 2018, **36**, 48–73, DOI: [10.1016/j.jphotochemrev.2018.07.001](https://doi.org/10.1016/j.jphotochemrev.2018.07.001).
- 26 D. D. Burns, K. L. Teppang, R. W. Lee, M. E. Lokensgard and B. W. Purse, Fluorescence Turn-On Sensing of DNA Duplex Formation by a Tricyclic Cytidine Analogue, *J. Am. Chem. Soc.*, 2017, **139**, 1372–1375, DOI: [10.1021/jacs.6b10410](https://doi.org/10.1021/jacs.6b10410).
- 27 K. L. Teppang, R. W. Lee, D. D. Burns, M. B. Turner, M. E. Lokensgard, A. L. Cooksy and B. W. Purse, Electronic Modifications of Fluorescent Cytidine Analogues Control Photophysics and Fluorescent Responses to Base Stacking and Pairing, *Chem. – Eur. J.*, 2019, **25**(5), 1249–1259, DOI: [10.1002/chem.201803653](https://doi.org/10.1002/chem.201803653).
- 28 G. N. Samaan, M. K. Wyllie, J. M. Cizmic, L.-M. Needham, D. Nobis, K. Ngo, S. Andersen, S. W. Magennis, S. F. Lee and B. W. Purse, Single-Molecule Fluorescence Detection of a Tricyclic Nucleoside Analogue, *Chem. Sci.*, 2021, **12**(7), 2623–2628, DOI: [10.1039/D0SC03903A](https://doi.org/10.1039/D0SC03903A).
- 29 G. N. Samaan, A. J. Salinas, A. E. Bailie, J. Grim, J. M. Cizmic, A. C. Jones, Y. Lee and B. W. Purse, Single-Molecule Detection of Oligonucleotides Using the Fluorescent Nucleobase Analogue ABN, *Chem. Sci.*, 2025, **16**(11), 4866–4875, DOI: [10.1039/D4SC07334G](https://doi.org/10.1039/D4SC07334G).
- 30 R. A. Mizrahi, D. Shin, R. W. Sinkeldam, K. J. Phelps, A. Fin, D. J. Tantillo, Y. Tor and P. A. Beal, A Fluorescent Adenosine Analogue as a Substrate for an A-to-I RNA Editing Enzyme, *Angew. Chem.*, 2015, **54**(30), 8713–8716, DOI: [10.1002/anie.201502070](https://doi.org/10.1002/anie.201502070).
- 31 P. Pfeiffer, J. R. Nilsson, A. Gallud, T. Baladi, H.-N. Le, M. Bood, M. Lemurell, A. Dahlén, M. Grøtli, E. K. Esbjörner and L. M. Wilhelmsson, Metabolic RNA Labeling in Non-Engineered Cells Following Spontaneous Uptake of Fluorescent Nucleoside Phosphate Analogues, *Nucleic Acids Res.*, 2024, **52**(17), 10102–10118, DOI: [10.1093/nar/gkac722](https://doi.org/10.1093/nar/gkac722).
- 32 T. L. Coulson and J. R. Widom, Impacts of Sequence and Structure on Pyrrolocytosine Fluorescence in RNA, *Nucleic Acids Res.*, 2025, **53**(7), gkaf262, DOI: [10.1093/nar/gkaf262](https://doi.org/10.1093/nar/gkaf262).
- 33 S. Poddar and M. Levitus, Quenching of 2-Aminopurine by Phosphates: Implications for Nucleic Acid Research, *Biophys. J.*, 2024, **123**(3), 495a, DOI: [10.1016/j.bpj.2023.11.2995](https://doi.org/10.1016/j.bpj.2023.11.2995).
- 34 J. Kuchlyan, L. Martinez-Fernandez, M. Mori, K. Gavvala, S. Ciaco, C. Boudier, L. Richert, P. Didier, Y. Tor, R. Improta and Y. Mély, What Makes Thienoguanosine an Outstanding Fluorescent DNA Probe?, *J. Am. Chem. Soc.*, 2020, **142**(40), 16999–17014, DOI: [10.1021/jacs.0c06165](https://doi.org/10.1021/jacs.0c06165).
- 35 L. M. Wilhelmsson, Fluorescent Nucleic Acid Base Analogues, *Q. Rev. Biophys.*, 2010, **43**(02), 159–183.
- 36 Y. Xie, T. Maxson and Y. Tor, Fluorescent Nucleoside Analogue Displays Enhanced Emission upon Pairing with Guanine, *Org. Biomol. Chem.*, 2010, **8**(22), 5053–5055, DOI: [10.1039/c0ob00413h](https://doi.org/10.1039/c0ob00413h).
- 37 R. W. Sinkeldam, A. J. Wheat, H. Boyaci and Y. Tor, Emissive Nucleosides as Molecular Rotors, *Chem. Phys. Chem.*, 2011, **12**(3), 567–570, DOI: [10.1002/cphc.201001002](https://doi.org/10.1002/cphc.201001002).
- 38 A. Karimi, R. Börner, G. Mata and N. W. Luedtke, A Highly Fluorescent Nucleobase Molecular Rotor, *J. Am. Chem. Soc.*, 2020, **142**(34), 14422–14426, DOI: [10.1021/jacs.0c05180](https://doi.org/10.1021/jacs.0c05180).
- 39 M. B. Turner, J. M. Cizmic, D. B. Rosansky, J. Ceja, M. Patterson, S. Kilcoyne, K. Thurber, G. Kim, T. J. Dwyer and B. W. Purse, Sequence-Specific Fluorescence Turn-On Sensing of RNA by DNA Probes Incorporating the Tricyclic Cytidine Analogue DEAtC, *Bioconjugate Chem.*, 2023, **34**(6), 1061–1071, DOI: [10.1021/acs.bioconjchem.3c00134](https://doi.org/10.1021/acs.bioconjchem.3c00134).
- 40 P. Sandin, K. Borjesson, H. Li, J. Martensson, T. Brown, L. M. Wilhelmsson and B. Albinsson, Characterization and Use of an Unprecedentedly Bright and Structurally Non-Perturbing Fluorescent DNA Base Analogue, *Nucleic Acids Res.*, 2008, **36**(1), 157–167.
- 41 A. F. Führtbauer, S. Preus, K. Börjesson, S. A. McPhee, D. M. J. Lilley and L. M. Wilhelmsson, Fluorescent RNA Cytosine Analogue – an Internal Probe for Detailed Structure and Dynamics Investigations, *Sci. Rep.*, 2017, **7**(1), 2393, DOI: [10.1038/s41598-017-02453-1](https://doi.org/10.1038/s41598-017-02453-1).
- 42 K. Börjesson, S. Preus, A. H. El-Sagheer, T. Brown, B. Albinsson and L. M. Wilhelmsson, Nucleic Acid Base Analog FRET-Pair Facilitating Detailed Structural Measurements in Nucleic Acid Containing Systems, *J. Am. Chem. Soc.*, 2009, **131**(12), 4288–4293.
- 43 J. N. Wilson, Y. Cho, S. Tan, A. Cuppoletti and E. T. Kool, Quenching of Fluorescent Nucleobases by Neighboring DNA: The “Insulator” Concept, *ChemBioChem*, 2008, **9**(2), 279–285.
- 44 P. Sandin, L. M. Wilhelmsson, P. Lincoln, V. E. C. Powers, T. Brown and B. Albinsson, Fluorescent Properties of DNA Base Analogue tC upon Incorporation into DNA-Negligible Influence of Neighbouring Bases on Fluorescence Quantum Yield, *Nucleic Acids Res.*, 2005, **33**(16), 5019–5025.
- 45 O. Tkach, L. Martinez-Fernandez, N. Humbert, L. Richert, D. Dziuba, P. Didier, Y. Tor, R. Improta and Y. Mély, Photophysical Characterization of Isothiazologuanosine, a Unique Isomorphous and Isofunctional Fluorescent Analogue of Guanosine, *J. Photochem. Photobiol., A*, 2024, **446**, 115075, DOI: [10.1016/j.jphotochem.2023.115075](https://doi.org/10.1016/j.jphotochem.2023.115075).
- 46 O. Tkach, L. Martinez-Fernandez, A. E. Ruiz-Lera, N. Humbert, L. Richert, D. Dziuba, E. Bombarda, A. Bourderieux, F. Hanser,



- P. Didier, Y. Tor, R. Improta, J. Léonard and Y. Mély, Exploring Excited-State Proton Transfer Reactions in Isothiazolobiosine, an Isofunctional Fluorescent Analogue of Guanosine, *Phys. Chem. Chem. Phys.*, 2025, 27(37), 19820–19836, DOI: [10.1039/D5CP02642C](https://doi.org/10.1039/D5CP02642C).
- 47 G. Stengel, B. W. Purse, L. M. Wilhelmsson, M. Urban and R. D. Kuchta, Ambivalent Incorporation of the Fluorescent Cytosine Analogues tC and tCo by Human DNA Polymerase  $\alpha$  and Klenow Fragment, *Biochemistry*, 2009, 48(31), 7547–7555.
- 48 N. J. Greco, R. W. Sinkeldam and Y. Tor, An Emissive C Analog Distinguishes between G, 8-oxoG, and T, *Org. Lett.*, 2009, 11(5), 1115–1118, DOI: [10.1021/ol802656n](https://doi.org/10.1021/ol802656n).
- 49 Y. Taniguchi, Y. Koga, K. Fukabori, R. Kawaguchi and S. Sasaki, OFF-to-ON Type Fluorescent Probe for the Detection of 8-Oxo-dG in DNA by the Adap-Masked ODN Probe, *Bioorg. Med. Chem. Lett.*, 2012, 22(1), 543–546, DOI: [10.1016/j.bmcl.2011.10.093](https://doi.org/10.1016/j.bmcl.2011.10.093).
- 50 A. D. Becke, Density-Functional Thermochemistry. III. The Role of Exact Exchange, *J. Chem. Phys.*, 1993, 98(7), 5648–5652, DOI: [10.1063/1.464913](https://doi.org/10.1063/1.464913).
- 51 C. Lee, W. Yang and R. G. Parr, Development of the Colle-Salvetti Correlation-Energy Formula into a Functional of the Electron Density, *Phys. Rev. B: Condens. Matter Mater. Phys.*, 1988, 37(2), 785–789, DOI: [10.1103/PhysRevB.37.785](https://doi.org/10.1103/PhysRevB.37.785).
- 52 D. G. A. Smith, L. A. Burns, K. Patkowski and C. D. Sherrill, Revised Damping Parameters for the D3 Dispersion Correction to Density Functional Theory, *J. Phys. Chem. Lett.*, 2016, 7(12), 2197–2203, DOI: [10.1021/acs.jpcclett.6b00780](https://doi.org/10.1021/acs.jpcclett.6b00780).
- 53 S. Grimme, S. Ehrlich and L. Goerigk, Effect of the Damping Function in Dispersion Corrected Density Functional Theory, *J. Comput. Chem.*, 2011, 32(7), 1456–1465, DOI: [10.1002/jcc.21759](https://doi.org/10.1002/jcc.21759).
- 54 R. A. Kendall, T. H. Dunning and R. J. Harrison, Electron Affinities of the First-Row Atoms Revisited. Systematic Basis Sets and Wave Functions, *J. Chem. Phys.*, 1992, 96(9), 6796–6806, DOI: [10.1063/1.462569](https://doi.org/10.1063/1.462569).
- 55 T. H. Dunning, Gaussian Basis Sets for Use in Correlated Molecular Calculations. I. The Atoms Boron through Neon and Hydrogen, *J. Chem. Phys.*, 1989, 90(2), 1007–1023, DOI: [10.1063/1.456153](https://doi.org/10.1063/1.456153).
- 56 A. V. Marenich, C. J. Cramer and D. G. Truhlar, Universal Solvation Model Based on Solute Electron Density and on a Continuum Model of the Solvent Defined by the Bulk Dielectric Constant and Atomic Surface Tensions, *J. Phys. Chem. B*, 2009, 113(18), 6378–6396, DOI: [10.1021/jp810292n](https://doi.org/10.1021/jp810292n).
- 57 T. Yanai, D. P. Tew and N. C. Handy, A New Hybrid Exchange–Correlation Functional Using the Coulomb-Attenuating Method (CAM-B3LYP), *Chem. Phys. Lett.*, 2004, 393(1–3), 51–57, DOI: [10.1016/j.cplett.2004.06.011](https://doi.org/10.1016/j.cplett.2004.06.011).
- 58 Y. Shao, Y. Mei, D. Sundholm and V. R. I. Kaila, Benchmarking the Performance of Time-Dependent Density Functional Theory Methods on Biochromophores, *J. Chem. Theory Comput.*, 2020, 16(1), 587–600, DOI: [10.1021/acs.jctc.9b00823](https://doi.org/10.1021/acs.jctc.9b00823).
- 59 J. Liang, X. Feng, D. Hait and M. Head-Gordon, Revisiting the Performance of Time-Dependent Density Functional Theory for Electronic Excitations: Assessment of 43 Popular and Recently Developed Functionals from Rungs One to Four, *J. Chem. Theory Comput.*, 2022, 18(6), 3460–3473, DOI: [10.1021/acs.jctc.2c00160](https://doi.org/10.1021/acs.jctc.2c00160).
- 60 N. Mardirossian and M. Head-Gordon, Thirty Years of Density Functional Theory in Computational Chemistry: An Overview and Extensive Assessment of 200 Density Functionals, *Mol. Phys.*, 2017, 115(19), 2315–2372, DOI: [10.1080/00268976.2017.1333644](https://doi.org/10.1080/00268976.2017.1333644).
- 61 A. Suzuki, M. Saito, R. Katoh and Y. Saito, Synthesis of 8-Aza-3,7-Dideaza-2'-Deoxyadenosines Possessing a New Adenosine Skeleton as an Environmentally Sensitive Fluorescent Nucleoside for Monitoring the DNA Minor Groove, *Org. Biomol. Chem.*, 2015, 13(27), 7459–7468, DOI: [10.1039/C5OB00862J](https://doi.org/10.1039/C5OB00862J).
- 62 T. J. Boerner; S. Deems; T. R. Furlani; S. L. Knuth and J. Towns, ACCESS: Advancing Innovation: NSF's Advanced Cyberinfrastructure Coordination Ecosystem: Services & Support, in *Practice and Experience in Advanced Research Computing 2023: Computing for the Common Good*; PEARC '23, Association for Computing Machinery, New York, NY, USA, 2023, pp. 173–176, DOI: [10.1145/3569951.3597559](https://doi.org/10.1145/3569951.3597559).

